PORE GEOMETRY AND PERMEABILITY MODELING FROM PRESSURE DEPENDENCE OF TRANSPORT PROPERTIES IN SANDSTONE

by

Yves Bernabé[1]

Department of Earth, Atmospheric, and Planetary Sciences
Massachusetts Institute of Technology
Cambridge, MA 02139

ABSTRACT

In this paper, a model of the pore geometry of sandstones is proposed. Three categories of pores are considered: large spherical pores at 4-grain vertices, tube-like throats at 3-grain edges and narrow sheet-like throats at 2-grain faces. Tube-like and sheet-like throats control the transport properties whereas nodal pores dominate the storing capacity. Tube-like throats tend to enhance permeability and improve accessibility to the storage pore space. Exploiting the fact that these different types of pores respond very differently to pressure, it is possible to evaluate the volume fraction of each category of pores in the framework of a simple capillary model. This approach was applied to data from the literature. Satisfactory fit was obtained for most of the sandstones considered. The exceptions seemed to be associated with high clay content which was not accounted for by the model.

INTRODUCTION

Traditionally, the use of pressure in experimental rock physics was restricted to the simulation of in situ conditions. Recently, attempts were made to exploit the fact that pores with different shapes are differently affected by pressure and to use the pressure dependence of the transport properties to constrain pore geometry models (Seeburger and Nur 1984; Yale, 1984; in sandstones; Doyen, 1987; Johnson and Manning, 1986; Bernabé, 1986, 1988; in crystalline rocks; see also Cheng and Toksöz, 1979).

If the pressure is kept in a range where the rock response is purely elastic, the pore network topology remains nearly unaltered. Therefore, relations between porosity and transport properties containing no hidden variables can be empirically determined for each rock. Relevant pore geometry parameters can then be calculated using an

[1]Now at: Chevron Oil Field Research Co., P.O. Box 446, La Habra, CA 90655-0446

appropriate permeability model. In this approach, each rock is treated on its own. In fact, it is necessary to do so because, as Thompson et al. (1987) pointed out, meaningful comparison of different rocks can only be made when the relevant pore parameters have been determined for each rock.

Among the transport properties models the simplest are the so-called capillary models, in which the pore space is replaced by a single "equivalent" conduit (Scheidegger, 1974). These models work best when the pores are all similar in shape and size, and when percolation effects are negligible (two-phase flow is a typical area for which capillary models are not suitable). Recently, capillary models were successfully applied to crystalline rocks which only contain sheet-like pores or cracks (Paterson, 1983; Walsh and Brace, 1984; Bernabé, 1986, 1988). Although capillary models are difficult to generalize to other rocks with a wide variety of pore shapes, their simplicity makes them highly desirable in practice.

In the present study, a model of the pore geometry of granular aggregates like sandstones is proposed. In sandstones, highly complex structures are associated with cement and clay (Thompson et al., 1987). Thus, as a start, I decided to restrict the model to clean sandstones (low clay content). Then, exploiting the fact that different types of pores respond differently to pressure, I attempted to adapt capillary models for use in materials with the assumed pore geometry. In this respect, a very helpful feature of sandstones was their broad elastic domain (for example, see Zhang et al., 1988).

PORE GEOMETRY MODEL

The pore geometry of sandstones has been extensively studied in the past with a wide range of techniques (for a review, see Dullien, 1979). Sandstones usually exhibit highly coordinated pore networks and rough pore/grain interfaces (Thompson et al., 1987). Caruso et al. (1985) examined rock sections and pore casts in the scanning electron microscope and distinguished three categories of pores: namely, intergranular pores (large, roughly equi-dimensional voids situated at 4-grain vertices, simply called "pores" or "nodal pores" in other studies), connective pores (very narrow, sheet-like pores situated along 2-grain faces, usually known as "throats"), and micropores (this term refers to the pore space left after filling up pores or throats with clay particles). Pores and throats have been recognized and used in models of transport and elastic properties for a long time (among others see Walsh and Brace, 1966, and more recently Yale, 1984, or Murphy et al., 1986). The throats control the transport properties whereas the nodal pores dominate the storage capacity.

As to the micropores, their tiny size renders detailed observation and modelling difficult. In most sandstones, clay particles are most likely found filling up nodal

pores. If the percentage of nodal pores free of clay is higher than a critical value which depends on the network topology, the transport properties are controlled by high conductivity flow paths passing round the clay filled pores. In that case the effect of micropores can be neglected.

In addition, studies of synthetic rock analogues suggest the possible existence of a second type of connective pore: namely, tubular conduits along 3-grain edges (Bernabé et al., 1982; Drory and Glaeser, 1985; Olgaard and Fitz Gerald, 1988). Although not easily distinguished in rock sections, these tube-like throats are observable in pore casts (Caruso et al., 1985). Their presence can enhance considerably permeability and improve the accessibility to storage pore space.

After these observations, the following pore geometry model was adopted: a highly coordinated network of sheet-like and tube-like throats connecting clay free spherical nodal pores (a similar model was used by Yale, 1984). These three categories of pores are not randomly distributed but arranged in a specific way as represented in Figure 1. According to this model, tube-like and sheet-like throats are *in parallel*, both forming connected sub-networks. Consequently, their contributions to hydraulic and electrical conduction are additive. Furthermore, the three categories of pores are very differently affected by pressure: sheet-like throats are compliant whereas tube-like throats and nodal pores are resistant to pressure (among others see Bernabé et al., 1982; Zimmerman, 1985). Therefore k, $1/F$ and ϕ can each be split into two terms: a pressure dependent term associated with the sheet-like throats and a pressure independent term associated with the tube-like throats and nodal pores.

$$k(P) = k_{tube} + k_{sheet}(P) \tag{1}$$

$$1/F(P) = 1/F_{tube} + 1/F_{sheet}(P) \tag{2}$$

$$\phi(P) = \phi_{node} + \phi_{tube} + \phi_{sheet}(P) \tag{3}$$

where P denotes the effective pressure (in absence of detailed experimental information, P is usually taken equal to the difference between the confining pressure P_c and the pore pressure P_p).

CAPILLARY MODEL

I will now review the capillary model used for crystalline rocks (Paterson, 1983; Walsh and Brace, 1984; Bernabé, 1986, 1988). The crack network is replaced by a single "equivalent" crack satisfying the following equations:

$$k_{crack} = w^2 \phi_{crack} / 12 \tau^2_{crack} \tag{4}$$

$$1/F_{crack} = \phi_{crack}/\tau^2_{crack} \tag{5}$$

$$\phi_{crack} = (w/2)(A_{crack}/V) \tag{6}$$

$$dw = -2^{2/3}h\ dP/P \tag{7}$$

where w is the width or aperture of the equivalent crack, τ_{crack} is the tortuosity, A_{crack} is the total wetted surface area of the cracks, V is the sample volume and h measures the roughness of the cracks (it is defined as the standard deviation of the asperity heights distribution; Brown and Scholz, 1985). Equation (4) is the usual Kozeny-Carman equation deduced from Darcy's law and Poiseuille flow equation for a flat crack. Two separate effects are corrected by the tortuosity factor: the cracks are inclined with respect to the macroscopic flow direction (geometric tortuosity), and the fluid has to flow around the asperities coming in contact as the crack closes (kinematic tortuosity). Notice that the geometric tortuosity is nearly constant while the kinematic tortuosity depends on pressure. Equation (5) is straightforwardly derived from Ohm's law. Strictly speaking, the tortuosity correction in (5) should not equal that in (4) as is implicitly assumed here. But it was found in the case of a single rough fracture that the ratio of the tortuosity factor for electric current to that for fluid flow was only slightly lower than one (Brown, 1989). Equation (6) simply expresses porosity as a function of crack aperture and specific wetted surface area of the cracks. Equation (7) gives the pressure dependence of the aperture of a nominally flat rough crack (Brown and Scholz, 1985).

Since k_{crack}, $1/F_{crack}$, ϕ_{crack}, w and τ_{crack} have to be expressed as a function of P, a fifth equation is needed. It can be chosen among the following 3 equivalent relations:

$$dk_{crack}/k_{crack} = Rd(1/F_{crack})/(1/F_{crack}) \tag{8}$$

$$d(1/F_{crack})/(1/F_{crack}) = Nd\phi_{crack}/\phi_{crack} \tag{9}$$

$$dk_{crack}/k_{crack} = Sd\phi_{crack}/\phi_{crack} \tag{10}$$

where the exponents R, N and S must be empirically determined and satisfy $S = RN$, and, using equations (4) to (6), $N = 2/(R-1)$. Bernabé (1988) simultaneously measured k and $1/F$ in Chelmsford granite and found $R \approx 2$. Values around 2 were also reported by Walsh and Brace (1984) for various crystalline rocks. Finally, $R \approx 2$ was obtained by Brown (1989) for a single rough fracture (his results showed only second order sensitivity to changes of the fractal dimension of the fracture walls). Assuming that the above model holds and $R = 2$, N and S must be equal to 2 and 4 respectively. Unfortunately, simultaneous measurements of the absolute values of ϕ and k or $1/F$ are very difficult to make under pressure in crystalline rocks. Consequently, the values of N and S mentioned above cannot be tested experimentally at the present time.

If $R = 2$, $N = 2$ and $S = 4$, it can be easily demonstrated that ($k_{crack}^{1/4}$, ($1/F_{crack}^{1/2}$ and ϕ_{crack} are proportional to the logarithm of P. These quantities form straight lines when plotted against P in a semi-log plot. The respective slopes A_k, $A_{1/F}$ and A_ϕ are given by:

$$A_k = -2^{3/4} h (A_{crack}/V)^{1/4} (3 w_0 \tau_0^2)^{-1/4} \tag{11}$$

$$A_{1/F} = -2h (A_{crack}/V)^{1/2} (w_0 \tau_0^2)^{-1/2} \tag{12}$$

$$A_\phi = -2^{1/2} h (A_{crack}/V) \tag{13}$$

where the subscript 0 refers to atmospheric pressure values. Knowing ϕ_0 and using equation (6), this system can be solved. In Chelmsford granite, Bernabé (1988) found reasonable values of h, w_0, τ_0 and A_{crack}/V (the last parameter was in excellent agreement with values independently measured using standard quantitative stereology methods).

In the case of sandstones, the capillary model approach can still be used, but provided that the complete combination of pores shown in Figure 1, instead of a single conduit, is considered "equivalent" to the pore network. The conditions for this approach to succeed are the following: a high coordination of the pore network and separately narrow size distributions of the conducting pores (sheet-like and tube-like throats). Thus, if k, $1/F$ and ϕ are partitioned as in equations (1), (2) and (3), the contribution of the sheet-like throats should obey the model described above (in other words, the subscript crack can simply be replaced in equations (4) to (13) by the subscript sheet). In particular, the exponents R_{sheet}, N_{sheet} and S_{sheet} must take the values 2, 2 and 4 respectively (as will be seen later, R, N and S calculated for the original data are generally not equal to 2, 2 and 4). Of course, the constant terms in the equations (1) to (3), k_{tube}, $1/F_{tube}$ and ϕ_{tube}, are not independent but satisfy the following equations similar to equations (4), (5) and (6):

$$k_{tube} = r 2 \phi_{tube} / 8 \tau_{tube}^2 \tag{14}$$

$$1/F_{tube} = \phi_{tube} / \tau_{tube}^2 \tag{15}$$

$$\phi_{tube} = \tau_{tube} \pi r^2 D \tag{16}$$

where r is the radius of the tube-like throats and D the tube density (the number of tube-like throats intersecting a unit area of rock section). D can possibly be measured independently from rock section micrographs. Notice that, according to the pore geometry model used here, the square root of $1/D$ should be approximately equal to the grain size. Knowing D and assuming a reasonable value for the geometric tortuosity τ_{tube}^2 (for instance 2, which corresponds to tubes inclined at 45° with respect to the

macroscopic flow direction), r can be eliminated from the above equations. Thus, the following trial and error procedure can be used to evaluate k_{tube}, $1/F_{tube}$, ϕ_{tube} and ϕ_{node}: k_{tube} is arbitrarily chosen, $1/F_{tube}$ and ϕ_{tube} are computed using equations (14) to (16), these three quantities are then substracted from $k(P)$, $1/F(P)$ and $\phi(P)$, and the exponent R_{sheet} is calculated. If R_{sheet} is not equal to 2, another value is tried for k_{tube} and the procedure is repeated. If Rsheet is equal to 2, ϕ_{node} is adjusted in order to finally obtain $N_{sheet} = 2$ and $S_{sheet} = 4$.

APPLICATION AND DISCUSSION

The procedure described above was applied to data from Fatt (1957), Wyble (1958), Dobrynin (1962), Chierici et al. (1967) and Yale (1984). 27 sandstones were selected from these studies (the digitized numerical values of k, F and ϕ were taken from Yale, 1984). This set of sandstones (see Table 1) covers wide ranges of porosity (from 1.9 to $2710^{-15}m^2$) and inverse formation factor (from 0.083 to 0.0014). For each rock, the exponents R, N and S were calculated (R varied from 0.45 to 7.26, N from 1.24 to 5.94 and S from 1.24 to 20.8). Low R's seemed weakly correlated to high permeabilities, and high S's to low permeabilities. Unfortunately, these studies did not include pore structure observations. In the absence of pore geometry data, an assumption had to be made for D. I tried 4 values corresponding to grain sizes most frequently observed in sandstones (namely 200, 100, 50 and 25 mm). The computations showed that, when the grain size was divided by 2, $1/F_{tube}$ and ϕ_{tube} increased by a factor slightly larger than 2, k_{tube} and ϕ_{node} also increased but very moderately and r decreased by a factor close to the square root of 2, which is consistent with the equations (14) to (16).

For 20 out of the 27 sandstones listed in Table 1, it was possible to find values of k_{tube}, $1/F_{tube}$, ϕ_{tube} and ϕ_{node} which yielded $R_{sheet} = 2$, $N_{sheet} = 2$ and $S_{sheet} = 4$. However, solutions were not always obtained for the 4 values of the grain size tried. The "best" or "sharpest" solutions (the ones for which the smallest change in k_{tube} produced the largest change in R_{sheet}) are given in Table 2. Figure 2 shows the curves $ln(k)$ versus $ln(1/F)$, $ln(1/F)$ versus $ln(\phi)$ and $ln(\phi)$ versus $ln(k)$ in Tertiary 807 for both the original and the treated data. These curves appear fairly linear, implying that equations (8) to (10) were satisfied in this rock. Acceptable linearity was observed for all the rocks, except maybe Triassic 38.

The 19 sandstones of Table 2 can be divided in two groups: 15 rocks with R's significantly lower than 2 and 4 with R's near 2 (corresponding to high values of S). As can be seen in Table 2, the first group is characterized by relatively high volume fraction of tube-like throats. In these rocks the permeability is generally high and the storing pore space is expected to be easily accessible. Therefore, the first group mainly contains good reservoir rocks. To the contrary, the second group is characterized by negligible tube volume fraction and corresponds to poor reservoir rocks.

Two samples, Massillon DV and Massillon DH, were cored from the same formation. DV means that the sample axis is vertical (or perpendicular to the bedding), while DH refers to horizontal axis (or parallel to the bedding). As can be seen in Table 1, Massillon sandstone is strongly anisotropic (Massillon DH is 20 times more permeable than Massillon DV). Interestingly enough, Massillon DV belongs to the first group whereas Massillon DH is included in the second. Anisotropy in sandstones is often due to layering as is schematically shown in Figure 3. One can see that the large tube-like throats in the high permeability layers control the transport properties in the direction parallel to these layers (or DH). But, the same tube-like throats appear as storing pores (included in ϕ_{node}) when the transport properties are measured in the direction perpendicular to the layers (or DV).

Equations (11), (12), (13) and (16) were then used to compute w_0, h, A_{sheet}/V and r. The results are given in Table 3 and seem generally reasonable (in the average, tube diameters were around 10 μm, and sheet-like throat widths around 5 μm). The computations showed that h and A_{sheet}/V decreased with increasing grain size whereas w_0 remained nearly unchanged.

But, the lack of information on the microstructure prohibited more thorough discussion. Important questions cannot be answered here. In particular, do the small values of r and w_0 in Falher 161, Falher 192, Branford and Massillon DV correspond to real features? Also, 3 rocks (Miocene 7, Cambrian 16 and Pliocene 41) displayed large values of w_0. Do these large apertures really indicate the presence of sub-macroscopic fractures? Qualitative agreement was found with Yale's results (he applied his model to 9 of the sandstones listed in Table 1; 1984). For the rocks which, here, were associated with large volume fraction of tubes, Yale found a significant proportion of high aspect ratio conduits. But, his approach generally yielded a much higher volume fraction of nodal pores than in this study.

Figure 4 shows the plots of $k^{1/4}$, $1/F^{1/2}$ and ϕ against $ln(P)$ for the same rock as in Figure 2 (Tertiary 807). Again, the curves are fairly linear in this rock. However, this feature was not shared by all the rocks (the quality of the linearity is indicated for each rock in Table 3). A possible explanation for the non-linear curves is that the sheet-like throats (situated at the grain contacts) may not be nominally flat (see Figure 5) and equation (7) may be not be satisfied.

Among the 8 remaining sandstones, 6 were characterized by R's significantly larger than 2 and very large values of S (Table 4), which suggested that these rocks belonged to the second group (poor reservoir rocks). The technique used here is conceptually equivalent to removing the high conductivity, tubular conduits from the pore network. Since permeability is more dependent on high conductivity channels than electrical resistivity, the procedure described earlier can only increase the exponent R. No solution can therefore be found for rocks whith R's larger than the maximum value allowed by the model (namely 2).

The question then becomes: why do these rocks have R's higher than 2? Modal analysis showed that the rocks from the Falher formation were strongly altered and had an unusually high clay content (Yale, 1984). Assuming that, in these rocks, the grains are all coated with clay particles, two effects are expected: a reduction of the pore dimensions accompanied by a decrease of both k and $1/F$, and an enhanced surface conduction causing an increase of $1/F$. Obviously, no great difficulty can arise from the first effect. But, the procedure described above cannot be successfully applied before the pressure independent term introduced in equation (2) by surface conduction is removed. The amount of the needed correction can be experimentally evaluated by measuring the electrical conductivity using several fluids of different salinity. This was apparently not done for the 6 rocks of Table 4 (Fatt, 1957; Wyble, 1958; Yale, 1984). However, since these rocks apparently belonged to the second group (poor reservoir rocks), $1/F$ could be arbitrarily corrected by the amount needed to obtain $R = 2$. Then, the usual procedure could be applied. As expected, wo was generally smaller than the values reported in Table 3.

The last 2 rocks, Pliocene 35 and Indiana DV, were unusual in that they had R's close to 2 and S's smaller than 4. Since the operation of substracting ϕ_{node} from $\phi(P)$ only decreases the exponent S, and since S was already smaller than the target value, no solution could be found. But, with no microstructure information available, it was impossible to find out why and where the model failed.

CONCLUSIONS

A pore geometry model was proposed for clean sandstones. This model was based on general microstructure observations. 3 categories of pores were considered: nodal pores, tube-like throats and sheet-like throats, arranged as in Figure 1. The throats control the transport properties while the nodal pores dominate the storage capacity. The sheet-like throats are very compliant whereas the tubes and nodes are virtually unaffected by pressure. These features were exploited in order to evaluate, for each rock, the volume fraction of each type of pore and appraise the rock reservoir properties. For that purpose, a simple capillary model was used, in which the complete combination of pores shown in Figure 1, instead of a single conduit, was considered "equivalent" to the pore network.

This approach was applied to data from the literature. The models appeared to fit the data well for most of the rocks considered. Particularly remarkable were the results obtained for anisotropic rocks and for rocks with unusually high clay content. Unfortunately, the lack of microstructure data prevented quantitative comparison of the predicted pore parameters to independently measured, equivalent geometric parameters.

In summary, the approach proposed here seems promising. Among other things, it may help detecting sub-macroscopic fractures in rock samples, and provide some insight for understanding the effect of clay content and anisotropy. Finally, this approach can be adapted for use with other rock properties such as acoustic wave velocities or attenuation.

ACKNOWLEDGEMENTS

This research was funded partially by the ARO grants DAAG 29-85-G-0011 and DAAG 29-85-K-0226, and partially under the Founding Members Program of the Earth Resources Laboratory (MIT).

REFERENCES

Bernabé, Y., Pore volume and transport properties changes during pressure cycling of several crystalline rocks, *Mech. Mater., 5,* 235–249, 1986.

Bernabé, Y., Comparison of the effective pressure law for permeability and resistivity formation factor in Chelmsford granite, *PAGEOPH, 127,* 607–625, 1988.

Bernabé, Y., W.F. Brace, and Evans, B., Permeability, porosity and pore geometry of hot-pressed calcite, *Mech. Mater., 1,* 173–183, 1982.

Brown, S.R., Transport of fluid and electric current through a single fracture, *J. Geophys. Res., in press,* 1989.

Brown, S.R., and Scholz, C.H., Closure of random elastic surfaces in contact, *J. Geophys. Res., 90,* 5531–5545, 1985.

Caruso, L., Simmons, G., and Wilkens, R., The physical properties of a set of sandstones — part 1: the samples, *Int. J. Rock Mech. Min. Sci. & Geomech. Abstr., 22,* 381–392, 1985.

Cheng, C.H., and Toksöz, M.N., Inversion of seismic velocities for the pore aspect ratio spectrum of a rock, *J. Geophys. Res., 84,* 7533–7543, 1979.

Chierici, G.L., Ciucci,G.M., Eva, F., and Long, G., Effect of the overburden pressure on some petrophysical parameters of reservoir rocks, *Proc. 7th. World Petrol. Cong., 2,* 309–338, 1967.

Dobrynin, V.M., Effect of overburden pressure on some properties of sandstones, *Soc. Petrol. Engrs. J., 2,* 360–366, 1962.

Doyen, P.M., Crack geometry in igneous rocks: a maximum entropy inversion of elastic and transport properties, *J. Geophys. Res., 92,* 8169–8181, 1987.

Drory, M.D., and Glaeser, A.M., The stability of pore channels: experimental observations, J. Am. Ceram. Soc., 68, 14–15, 1985.

Dullien, F.A.L., *Porous Media: Fluid Transport and Pore Structure,* Academic Press, New York, pp. 396, 1979.

Fatt, I., Effect of overburden and reservoir pressure on electric logging formation factor, *Bull. Amer. Ass. Petrol. Geol., 41,* 2456–2466, 1957.

Johnson, D.L., and Manning, H.J., Theory of pressure dependent resistivity in crystalline rocks, *J. Geophys. Res., 91,* 11611–11617, 1986.

Murphy, W.F., Winkler, K.W., and Kleinberg, R.L., Acoustic relaxation in sedimentary rocks: dependence on grain contacts and fluid saturation, *Geophysics, 51,* 757–766, 1986.

Olgaard, D.L., and Fitz Gerald, J.D., Interface healing in synthetic marbles: a SEM/TEM study (abstr.), *Trans. Am. Geophys. Union, 69,* 1446, 1988.

Paterson, M.S., The equivalent channel model for permeability and resistivity in fluid-saturated rock — a re-appraisal, *Mech. Mater., 2,* 345–352, 1984.

Scheidegger, A.E., The Physics of Flow through Porous Media, Univ. of Toronto, Toronto, Ont., pp. 353, 1974.

Seeburger, D.A., and Nur, A., A pore space model for rock permeability and bulk modulus, *J. Geophys. Res., 89,* 527–536, 1984.

Thompson, A.H., Katz, A.J., and Krohn, C.E., The microgeometry and transport properties of sedimentary rock, *Advance in Phys., 36* 625–694, 1987.

Walsh, J.B., and Brace, W.F., Cracks and pores in rocks, in *Proc. Int. Congr. of Rock Mech., Lisbon,* 643–646, 1966.

Walsh, J.B., and Brace, W.B., The effect of pressure on porosity and the transport properties of rock, *J. Geophys. Res., 89,* 9425–9431, 1984.

Wyble, D.O., Effect of applied pressure on the conductivity, porosity and permeability of sandstones,*Trans. AIME, 213,* 430–432, 1958.

Yale, D.P., Network Modelling of Flow, Storage and Deformation in Porous Rocks, Ph.D. Thesis, Stanford Univ., Stanford, Calif., 1984.

Zhang, J., Wong, T.-F., and Davis, D.M., Hydrostatic compaction of porous rock and fracture mechanics analysis of grain crushing (abstr.), *Trans. Am. Geophys. Union, 69,* 1464, 1988.

Zimmerman, R.W., Compressibility of an isolated spheroidal cavity in an isotropic elastic medium, *J. Appl. Mech., 52,* 606–608, 1985.

Sample	k_{max}	$1/F_{max}$	ϕ_{max}	R	N	S	P_{min}	P_{max}
Berea 500[5]	490.	50.	20.	0.45	5.94	73.09	1.	49.
Cambrian 14[4]	32.	19.	11.	0.53	3.19	1.74	0.1	45.
Cambrian 6[4]	23.	11.	8.1	0.59	3.51	2.08	0.1	45.
Triassic 34[4]	350.	72.	20.	0.80	1.52	1.24	0.1	45.
Tertiary 807[5]	150.	67.	22.	0.82	3.23	2.65	1.	37.
Boise[5]	900.	83.	26.	0.84	3.14	2.77	1.	46.
Triassic 38[4]	400.	79.	21.	0.87	1.79	1.77	0.1	45
Massillon DH[5]	130.	42.	16.	0.94	2.78	2.68	1.	47.
Berea 100H[5]	49.	58.	17.	1.01	2.01	2.14	2.	46.
Miocene 7[4]	4.4	2.6	8.3	1.05	2.50	2.62	0.1	45.
Cambrian 16[4]	9.5	3.2	14.	1.17	3.23	3.79	0.1	45.
Triassic 26[4]	68.	58.	18.	1.29	2.10	2.78	0.1	45.
Fahler 161[5]	0.01	2.4	2.3	1.29	3.31	4.26	2.5	31.
Pliocene 41[4]	42.	6.9	21.	1.56	2.42	3.82	0.1	45.
Triassic 27[4]	72.	50.	18.	1.59	1.75	2.81	0.1	45.
Torpedo[3]	45.	24.	20.	1.78	4.02	7.56	0.1	99.
Branford[2]	2.5	11.	11.	1.86	3.32	6.22	0.1	34.
Pliocene 35[4]	37.	6.4	20.	1.93	1.59	3.17	0.1	45.
Massillon DV[5]	6.9	36.	19.	1.94	4.61	9.09	2.	47.
Indiana DV[5]	30.	83.	27.	1.98	1.24	2.73	1.	47.
Fahler 19[5]	0.007	3.8	4.6	2.22	2.89	6.64	2.5	31.
Kirkwood[2]	12.	25.	15.	2.40	3.79	9.12	0.1	34.
Tensleep[1]	120.	53.	15.	2.73	5.69	15.7	0.1	34.
Fahler 162[5]	0.27	3.4	3.0	2.76	3.47	9.70	2.5	31.
Fahler 189[5]	0.02	1.4	1.9	3.01	2.36	7.36	2.5	31.
Fahler 154[5]	0.009	7.8	4.4	3.05	3.51	10.7	2.5	31.
Fahler 142[5]	0.02	6.1	7.6	7.26	2.86	20.8	2.5	31.

Table 1: The sandstones considered in this study ([1] Fatt, 1957; [2] Wyble, 1958; [3] Dobrynin, 1962; [4] Chierici et al., 1967; [5] Yale, 1984). Permeabilities are in 10^{-15}m^2 or md, porosities in % and pressures in MPa. The values of the inverse formation factor must be multiplied by 10^{-3}.

Sample	k_{tube}	$1/F_{tube}$	ϕ_{tube}	ϕ_{node}	grain size
Berea 500	80	26	13	63	200
Cambrian 14	79	35	12	47	100
Cambrian 6	73	25	7	49	200
Triassic34	84	64	46	8	50
Tertiary 807	73	42	25	38	50
Boise	73	41	26	37	100
Triassic 38	80	60	45	12	50
Massillon DH	62	28	15	34	100
Berea 100H	61	25	17	12	50
Miocene 7	65	43	3	53	200
Cambrian 16	63	51	2	67	200
Triassic26	49	26	17	12	50
Fahler 161	22	10	2	39	25
Pliocene 41	42	41	3	51	200
Triassic 27	40	29	16	4	50
Torpedo	24	18	4	58	100
Branford	16	15	3	44	50
Massillon DV	20	18	7	58	25
Fahler 192	0	0	0	35	

Table 2: The set of sandstones for which solutions were obtained. k_{tube}, $1/F_{tube}$, ϕ_{tube} and ϕ_{node} are given in % of k_{max}, $1/F_{max}$ and ϕ_{max} respectively. The values of grain size are in μm.

Sample		grain size	$2r$	w_0	A_{sheet}/V	h
Berea 500	P	200	30.	5.8	130	95
Cambrian 14	P	100	11.	5.1	330	18
Cambrian 6	P	200	14.	5.2	240	18
Triassic 34	P	50	14.	7.1	440	25
Tertiary 807	G	50	11.	3.6	430	49
Boise	G	100	24.	7.2	240	46
Triassic 38	P	50	15.	6.0	330	29
Massillon DH	G	100	15.	5.7	370	28
Berea 100H	G	50	8.2	3.6	910	14
Miocene 7	P	200	9.0	41.	220	33
Cambrian 16	P	200	11.	63.	160	69
Triassic 26	P	50	8.4	4.3	840	11
Fahler 161	G	25	0.6	0.8	1000	16
Pliocene 41	P	200	14.	91.	270	63
Triassic 27	P	50	8.0	7.3	790	11
Torpedo	P	100	9.0	8.8	330	23
Branford	P	50	2.8	1.4	750	20
Massillon DV	G	25	2.6	1.9	840	19
Fahler 192	G		0.0	0.8	3400	6

Table 3: The pore parameters computed for the set of sandstones of Table 2. The grain size, the tube diameter $2r$ and the crack aperture w_0 are in μm, the specific wetted surface area of the sheet-like throats A_{sheet}/V is in cm^{-1} and the standard deviation of the asperity heights h is in $10^{-3}\mu m$. The letters G and P refer to good and poor linearity of the curves $k^{1/4}$ versus $ln(P)$, $1/F^{1/2}$ versus $ln(P)$ and ϕ versus $ln(P)$.

Sample		Corr. $(1/F)$	ϕ_{node}	w_0	A_{sheet}/V	h
Kirkwood	P	15	65	5.7	460	30
Tensleep	P	28	73	2.6	120	18
Falher 162	G	15	48	3.2	240	69
Falher 189	G	21	37	3.0	430	25
Falher 154	G	13	55	0.3	2400	8
Falher 142	G	57	75	1.3	1100	19

Table 4: The set of sandstones for which the inverse formation factor requires a correction (given here in % of $1/F_{max}$). The other units are the same as in previous Tables. The letters G and P have the same meaning as in Table 3.

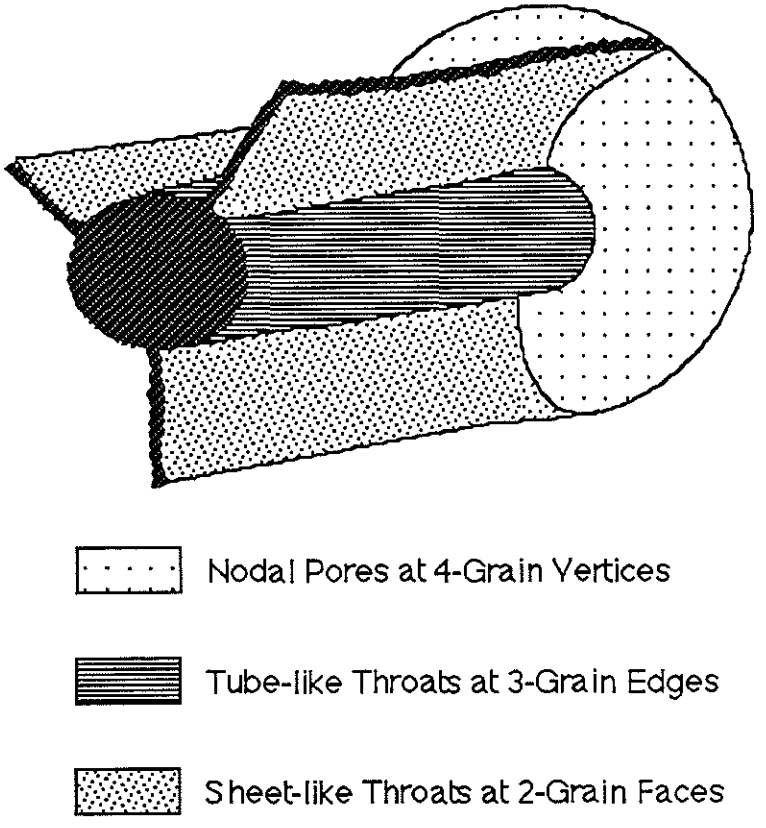

Figure 1: A schematic representation of the pore geometry of clean sandstones.

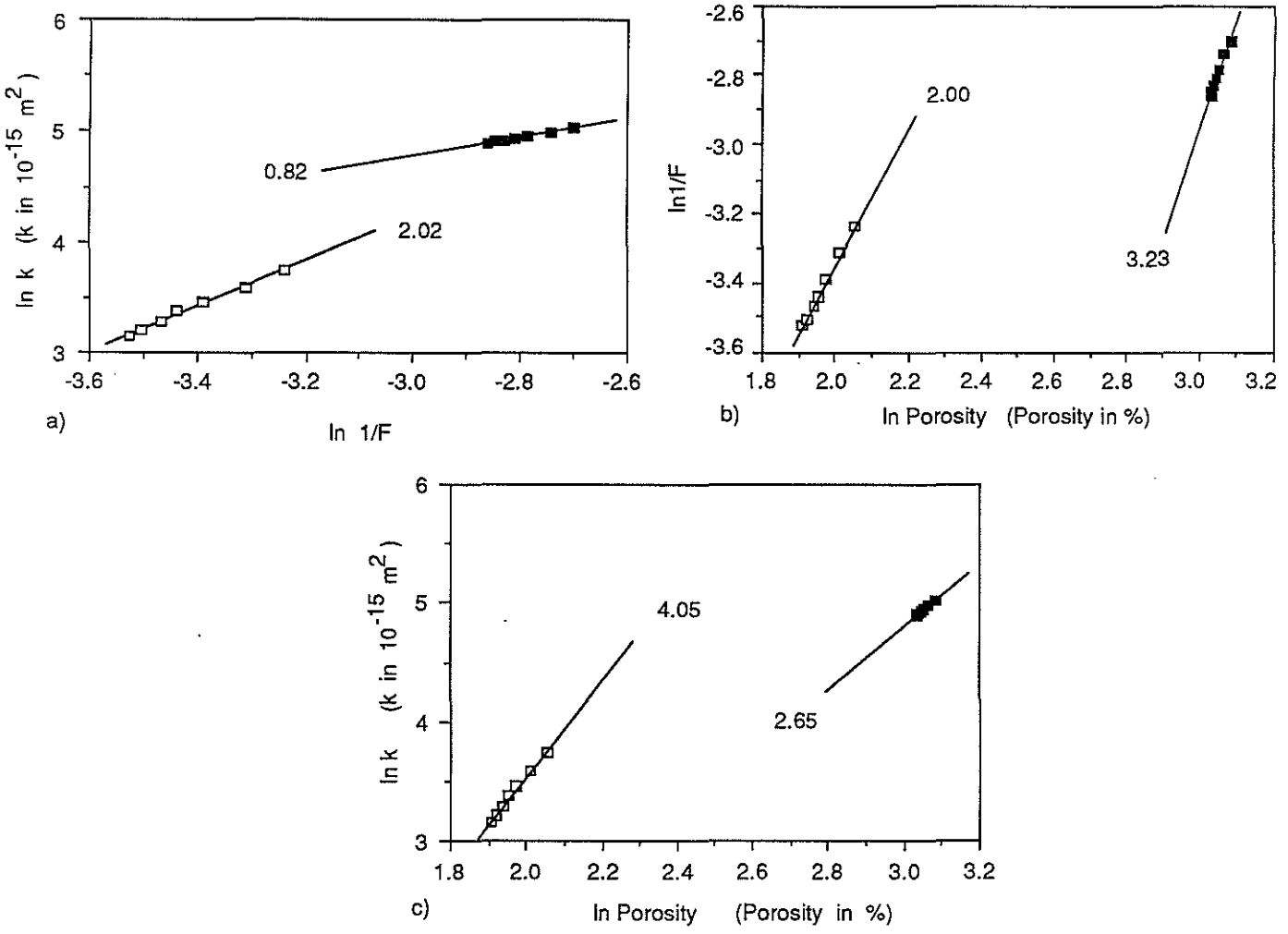

Figure 2: The curves $ln(k)$ versus $ln(1/F)$, $ln(1/F)$ versus $ln(\phi)$ and $ln(k)$ versus $ln(\phi)$ for Tertiary 807. The original data are represented by solid squares, and the treated data (k_{sheet}, $1/F_{sheet}$ and ϕ_{sheet}) by open squares. Best fit straight lines and the corresponding exponents R, N, S, R_{sheet}, N_{sheet} and S_{sheet} are also indicated.

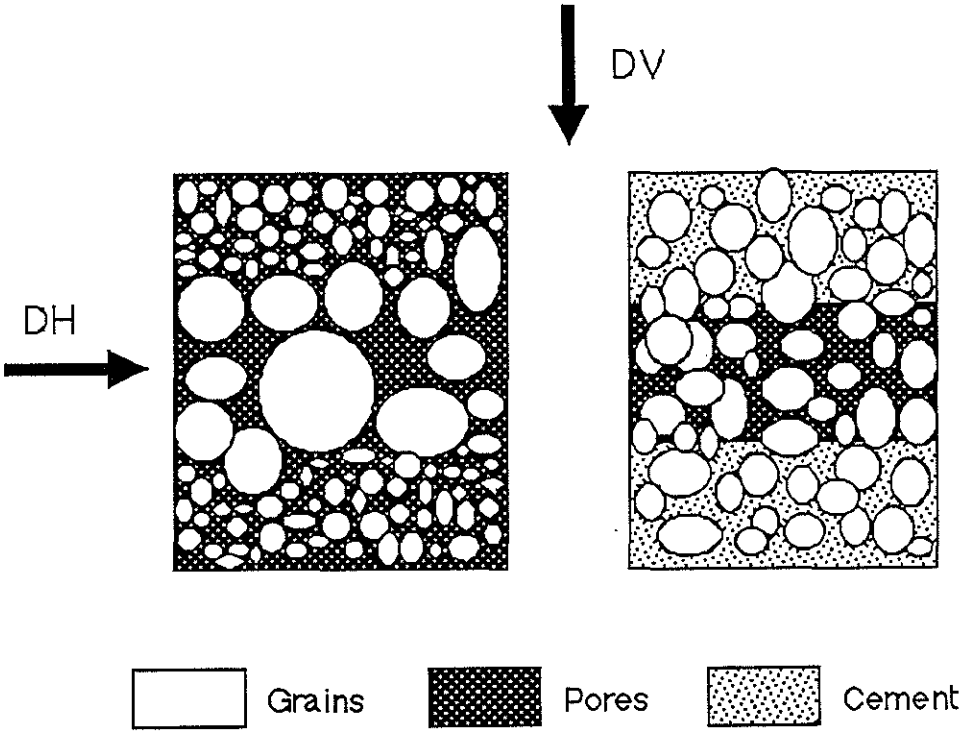

Figure 3: Two possible models of anisotropy in sandstones (left: layers of grains with different sizes; right: layers with different degree of cementation). The directions DV and DH are also indicated.

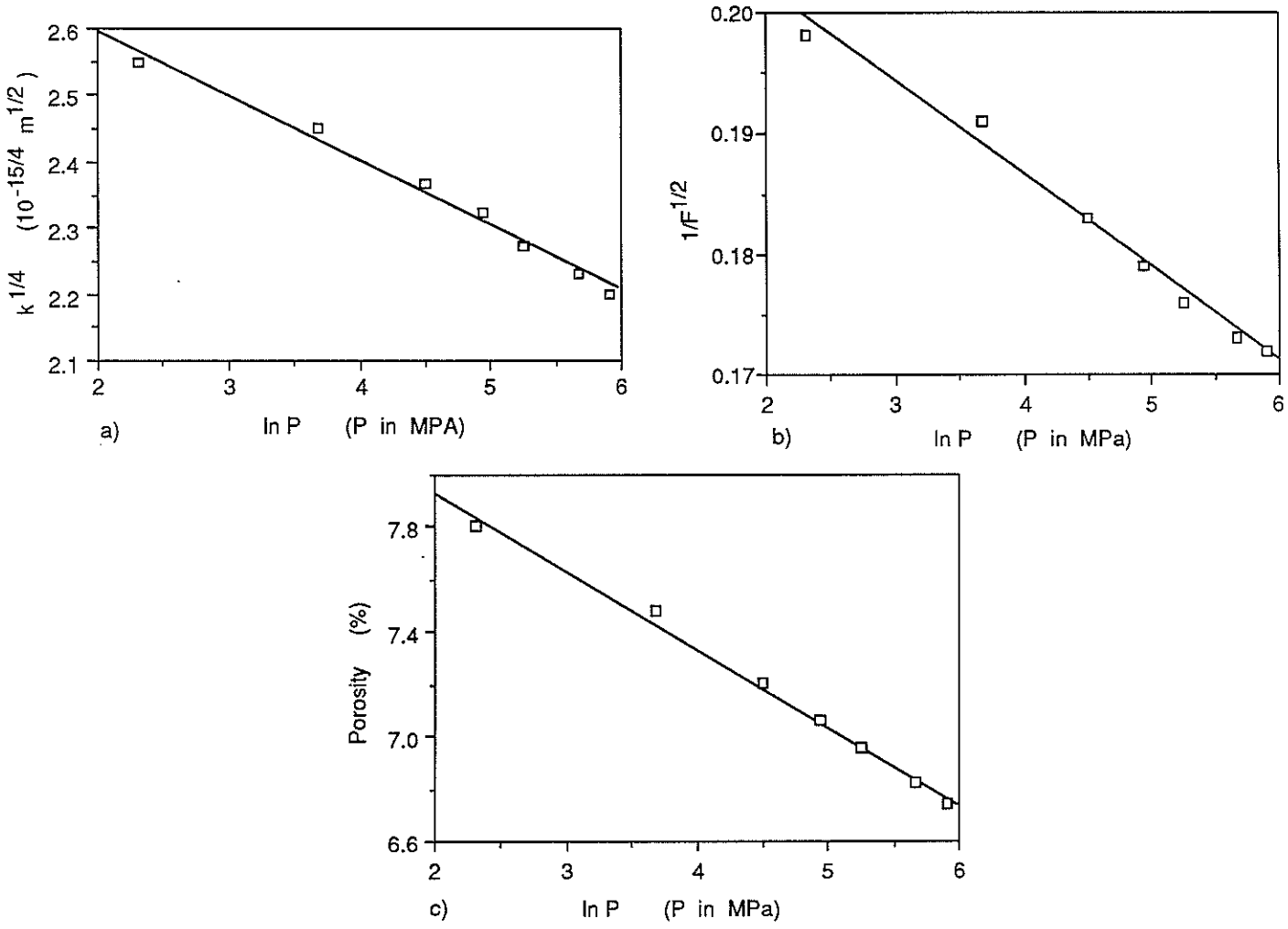

Figure 4: The curves $k_{sheet}^{1/4}$ versus $ln(P)$, $1/F_{sheet}^{1/2}$ versus $ln(P)$ and ϕ_{sheet} versus $ln(P)$ for Tertiary 807. Best fit straight lines are also plotted.

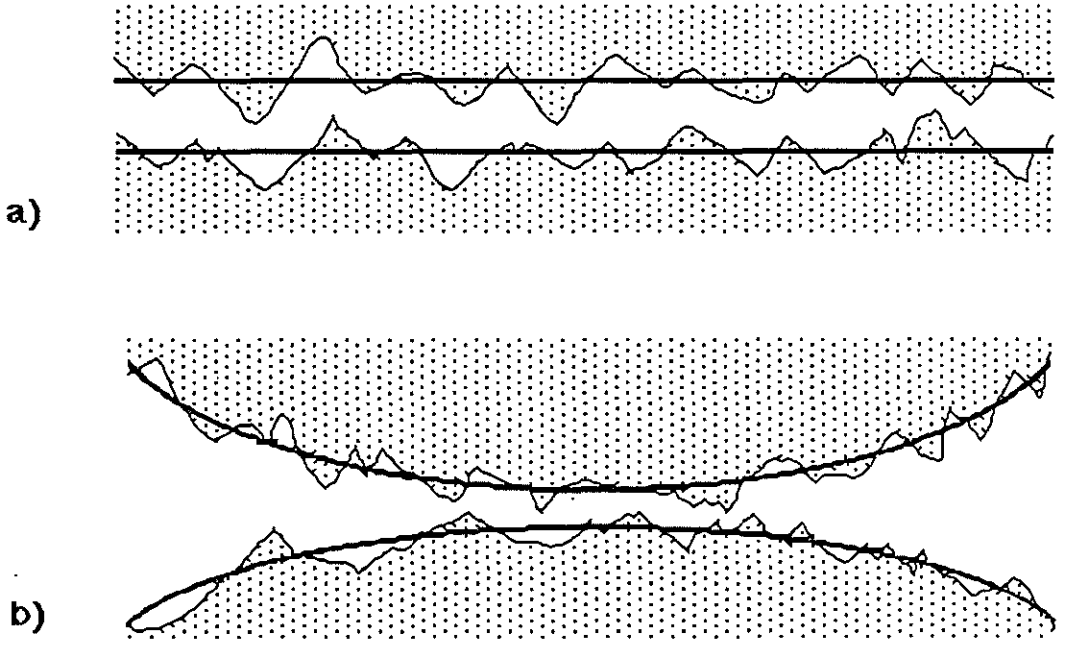

Figure 5: An illustration of the difference between flat sheet-like throats for which equation (7) applies and concave grain contact for which equation (7) is not satisfied. Notice that the roughness of the grains in this diagram is not realistically represented.